The growth mechanism and characterization of few-layer diphenyl dinaphthothienothiophene films prepared by vacuum deposition

Hattori, Yoshiaki
Kimura, Yoshinari
Yoshioka, Takumi
Kitamura, Masatoshi

(Citation)
Organic Electronics,74:245-250

(Issue Date)
2019-11

(Resource Type)
journal article

(Version)
Accepted Manuscript

(URL)
https://hdl.handle.net/20.500.14094/90006424

The Growth Mechanism and Characterization of Few-layer Diphenyl Dinaphthothienothiophene Films Prepared by Vacuum Deposition

Yoshiaki Hattori[*]*, Yoshinari Kimura, Takumi Yoshioka, and Masatoshi Kitamura*[**]

Department of Electrical and Electronic Engineering, Kobe University, 1-1, Rokkodai-cho, Nada-ku, Kobe, 657-8501, Japan

Corresponding Author

Email: [*]hattori@eedept.kobe-u.ac.jp, [**]kitamura@eedept.kobe-u.ac.jp

Keywords:

DPh-DNTT, layer-by-layer growth, vacuum deposition, 2D island, fractal.

ABSTRACT:

The growth mechanism of 2,9-diphenyl-dinaphtho[2,3-*b*:2',3'-*f*]thieno[3,2-*b*]thiophene (DPh-DNTT) thin-films prepared by vacuum deposition was investigated based on the morphological crystallinity of the obtained films. In addition to atomic force microscopy, which is commonly used for imaging surface morphology, optical microscopy was also positively used for the same purpose. The technique allows the quick and easy evaluation of thin films. The optical microscopy images show that DPh-DNTT films grew according to a layer-by-layer growth mode. Each layer grew as flat two-dimensional (2D) islands with a thickness of about 2.3 nm, where DPh-DNTT molecules stand almost vertically with respect to the –layer below. The height difference between layers provided a color contrast in these images, which visualizes the initial 2D island on the SiO_2 substrate and fractal-shape 2D islands on top surface. By using the method, a monolayer of isolated and round 2D islands, with a diameter of approximately 4 μm, formed at a high substrate temperature on a SiO_2 surface that had been previously treated with O_2 plasma or UV-O_3. The presence of a DPh-DNTT layer on the substrate was also confirmed by micro-Raman measurement.

INTORODUCTION

Organic semiconductors based on the dinaphtho[2,3-*b*:2',3'-*f*]thieno[3,2-*b*]thiophene (DNTT) series, including the didecyl (C_{10}-DNTT) and diphenyl derivatives (DPh-DNTT), have attracted wide attention as promising materials for electronic applications. Thin-films made of these organic semiconductors exhibit a high carrier mobility, heat-resistance [1, 2], and stability in air [2, 3] as compared to pentacene, which is a standard organic semiconductor. The carrier mobility in field-effect transistors (FETs) based on single-crystalline and polycrystalline DNTT can be as high as approximately 9 [4, 5] and 2 $cm^2\ V^{-1}\ s^{-1}$ [6, 7], respectively. The use of alkylated DNTT leads to an improvement in carrier mobility due to enhanced orbital coupling between neighboring molecules [8]. Indeed, FETs made of single-crystalline and polycrystalline C_{10}-DNTT exhibit field-effect mobilities of approximately 12 [9–11] and 8.3 $cm^2\ V^{-1}\ s^{-1}$ [3, 12–14], respectively. In addition, the high solubility of the alkylated derivative allows the formation of single-crystalline films from a solution [10–12, 15]. On the other hand, the diphenyl derivative has a lower solubility, and the carrier mobility in polycrystalline DPh-DNTT films is approximately 3 to 5 $cm^2\ V^{-1}\ s^{-1}$ [2, 14, 16], which is lower than that in C_{10}-DNTT films. The advantage of DPh-DNTT resides in its thermal stability. In fact, DPh-DNTT FETs can work even at 250 °C [1, 2]. In addition, researchers have reported that carrier mobility in DPh-DNTT films is less affected by the specifics of the device structure, as compared to C_{10}-DNTT films [16]. This suggests that DPh-DNTT is more suitable than C_{10}-DNTT for applications to the actual device structure that includes bottom gate on rough substrates.

Vacuum deposition is the main method used for the preparation of organic thin films and allows to obtain large and uniform films regardless of the solubility of the organic materials. In addition, this method is applicable to the deposition of organic materials on rough substrates such as plastic films and printed papers for flexible electronics. Carrier mobility is

determined by the crystallinity or the morphology of the deposited organic films. Furthermore, the carrier mobility in the deposited organic films depends on the device structure [1, 5, 16–18], underlayer materials [4, 8, 19], surface treatments [2, 3, 6, 15], and substrate temperature [2, 3, 6, 12].

The morphology of DNTT-series-based thin films has been investigated by atomic force microscopy (AFM) [10, 12, 16, 17, 20] and scanning electron microscopy (SEM) [12, 16]. DNTT, C_{10}-DNTT, and DPh-DNTT molecules crystallize in a herringbone packing arrangement in both the bulk [2, 4] and thin films [2]. Step-terrace structures have been observed in vacuum-deposited DNTT [4, 16] and C_{10}-DNTT [12] films deposited under certain conditions. The feature of the vacuum-deposited film is tall walls that protrude from the surface [12, 18]. Such three-dimensional structures with large irregularities prevent the observation of the surface by AFM. Since carrier transport in FETs takes place within the few-nanometer region close to the interface between the organic film and the gate insulator [21], observation of the initial stages of growth on the gate insulator is important. Therefore, the initial stages of growth of organic films prepared by vacuum deposition have been extensively studied using pentacene [21–37]. On the other hand, the initial stages of growth for DNTT-series-based films have not been sufficiently studied, although there are a few literatures on the initial growth of DNTT [20]. Thus, conducting a systematic observation to elucidate the growth mechanism of these films to ultimately improve FET performance is necessary.

In this study, the morphology of few-nanometer-thick 2,9-diphenyl-dinaphtho[2,3-*b*:2',3'-*f*]thieno[3,2-*b*]thiophene films was investigated by AFM, optical microscopy and micro-Raman. In addition, the initial stage of film formation and the nucleation density (N) of film islands were also studied. Although AFM measurements are generally used for this purpose [10, 12, 16, 17, 22–30], an optical microscope was positively used for the same

purpose. The observation by optical microscopy allows a quick and easy evaluation of the thin films. In order to be able to perform evaluations by optical microscopy, the following aspects must be met: (1) SiO_2 substrates with a thickness suitable for detecting the thin film deposited must be used; due to an optical interference effect, color contrast is maximized at a thickness of approximately 90 and 300 nm [38]; (2) The two-dimensional (2D) DPh-DNTT islands must be sufficiently thick, for enhanced image color contrast; (3) The size of the 2D islands must be larger than the resolution of the optical microscope; (4) DPh-DNTT films must grow according to a layer-by-layer mode, which gives a clear color contrast between the different layers; (5) Dark-field images must be recorded, which allows to measure N up to about 2.5 μm^{-2} using a standard optical microscope. The effects of the substrate temperature (T_s) and pre-treatment of the SiO_2 substrate surface on layer growth when using the vacuum deposition method is also discussed. In addition, the Raman spectra recorded for DPh-DNTT films deposited on the SiO_2 substrate confirmed the presence of DPh-DNTT.

EXPERIMENTAL SECTION

DPh-DNTT films were deposited on thermally grown SiO_2 (40- or 90-nm-thick) substrates. The thermal sublimation was conducted at a pressure of the order of 10^{-4} Pa with a deposition rate of 0.05 Å/s, which was monitored using a quartz crystal microbalance (QCM). Film thickness during the process was measured with the QCM as nominal film thickness. In order to examine the influence of the surface condition, four types of surface treatments were applied: (A) substrates were cleaned by sonication in acetone for 10 min, followed by cleaning in isopropanol (IPA) for 10 min; (B) substrates were cleaned with acetone and IPA and then exposed to UV-O_3 for 30 min; (C) substrates were cleaned with acetone and IPA and then exposed to oxygen plasma for 120 s (AC power for plasma

generation was set at 5.4 W); (D) substrates were cleaned with acetone and IPA and then exposed to UV-O_3 for 15 min, and finally the substrates were exposed to hexamethyldisilazane (HMDS) vapor at 120 °C for 1 hour. A detailed experimental procedure for the surface treatment is provided in our previous paper [39]. After surface treatment, the substrates were immediately placed in a vacuum chamber for the thermal sublimation step. Before starting the deposition of DPh-DNTT, substrates were heated to a target temperature and then kept at that temperature for longer than 20 min to degas and to achieve thermal equilibrium.

The deposited thin films were observed with an optical microscope (LV100, Nikon) equipped with a digital camera (EOS Kiss X4, Canon) [40]. Objective lenses with magnifications of 100x (LU Plan 100x/0.9, Nikon) and 150x (LU Plan Apo 150x/0.90, Nikon) were used. The morphological study was performed by AFM in tapping mode. The curvature of the AFM cantilever was 20 nm. The island nucleation density was estimated by counting the number of islands (at least 150 islands) in a certain area and dividing it by this area. A Raman spectroscopy system equipped with a 532-nm laser (5.3 mW) was used to characterize the DPh-DNTT films.

RESULTS AND DISCUSSION

The optical dark-field microscopy and AFM images in **Fig. 1** show 2D islands deposited at 160 °C on surfaces previously submitted to different treatments. The images in **Fig. 1(a–c)** show the growth evolution of a DPh-DNTT layer deposited on a substrate cleaned with acetone/IPA for a nominal film thickness of 1.2 nm **Fig. 1(a, b)** and 2.4 nm **Fig. 1(c)**. AFM image in **Fig. 1(b)** is the observation of the same sample for **Fig. 1(a)**. The sample for **Fig. 1(c)** is different. In both AFM images **Fig. 1(b−c)**, 2D islands with a height of 2.3 nm can be

seen on the surface. The fact that the height of the islands is close to the length of the longer axis of the DPh-DNTT molecule (~2.42 nm) [4] suggests that the molecules stand almost vertically with respect to the substrate in a herringbone packing arrangement, as revealed by X-ray diffraction images [2]. Although enough DPh-DNTT molecules were provided to complete one layer on the substrate surface, the first layer was incomplete, as shown in **Fig. 1(c)**, suggesting that desorption occurs during deposition [22, 23]. In fact, 160 °C is close to the upper T_s limit (~190°C) to form a DPh-DNTT film. Upon comparing both AFM images **Fig. 1(b-c)**, the area covered by 2D islands in **Fig. 1(c)** is clearly larger, where the relative size of each of 2D island in the same sample is almost the same. If the N increases with an increase of nominal thickness, tiny 2D islands should be observed in **Fig. 1(c)**. However, the morphology wasn't observed in the samples with the nominal thickness of less than ~3 nm regardless of the surface treatment and T_s. Therefore, the 2D islands must grow isotropically without any new nucleation. Note that N of **Fig. 1(c)** is higher than that of **Fig. 1(b)**. However, the difference is in the experimental error, which will be discussed later in **Fig. 2**. From the discussion, it is thought that N for **Fig. 1(b)** reached saturation. The growth behavior allows easy evaluation of N by optical microscopy.

The images in **Fig. 1(d–f)** correspond to the 2D islands deposited on the substrates treated with UV-O_3 **Fig. 1(d)**, O_2 plasma **Fig. 1(e)**, and HMDS **Fig. 1(f)**, respectively. The nominal thickness of the samples is 1.2 nm, which is comparable to that of the samples in **Fig. 1(a, b)**. The 2D islands deposited on the substrates treated with UV-O_3 or O_2 plasma are larger than those deposited on the substrate treated with HMDS [24, 30]. Therefore, pre-treatment of the substrates with UV-O_3 and O_2 plasma decreases N for the 2D islands. The change is attributed to the modification of the SiO_2 surface, not the degree of cleanliness. In comparison to the substrate cleaned with acetone/IPA, the HMDS treatment make the SiO_2 surface hydrophobic. While, UV-O_3 or O_2 plasma treatment change the surface to hydrophilic.

Quantitatively, the change can be evaluated as surface energy, and the correlation between surface energy and morphology of organic thin film as well as surface roughness and materials has been reported [23, 31].

The N for each surface treatment are shown in **Fig. 2** as a function of the inverse T_s. The N value decreases as T_s increases irrespective of surface treatment, resulting in the formation of large islands. Since the log(N) versus $1/T_s$ plot is a straight line, N can be expressed by an equation derived from nucleation rate equations as follows [41]:

$$N = A\exp(E_{nucl}/kT_s),$$

where k is the Boltzmann's constant, A is a constant, and E_{nucl} is the activation energy for homogeneous nucleation. The treatment of the SiO_2 surface can potentially affect the A and E_{nucl} values. From the slope in the figure, E_{nucl} for treatment of HMDS, acetone/IPA, UV-O_3, and O_2 plasma is calculated to be 0.32, 0.47, 0.66, and 0.71 eV, respectively. These value are comparable to that of pentacene [22, 23, 25], indicating the similarity of nucleation from the view point of activation energy. In addition, the effect of admolecular dynamics must be taken into account. According to the standard nucleation theory, N decreases as the surface diffusion constant (D_s) increases [41–43]. D_s can be expressed as follows:

$$D_s = D_0\exp(-E_{diff}/kT_s),$$

where D_0 is a constant, and E_{diff} is the activation energy for monomer diffusion [22, 44]. Note that the relationship between E_{nucl} and E_{diff} is shown in the references [22, 23]. Thus, the possibility exists that treatment of the SiO_2 substrate with UV-O_3 and O_2 plasma activates the dynamics of the admolecules, resulting in a reduced N value for the 2D islands.

Subsequently, the characteristics of the DPh-DNTT 2D islands were evaluated in relation to well-studied pentacene. The relationship between N and T_s for DPh-DNTT is similar to that of pentacene [22, 23, 25–29], although the experimental T_s range was different. The reported N for pentacene is 0.2 to 200 μm^{-2} in the T_s range of 20 °C to 70 °C, and the N

value in this study is of the same order. Therefore, the nucleation mechanism for pentacene may be applicable to DPh-DNTT. Regarding the shape of the 2D islands, pentacene 2D islands deposited on a SiO_2 substrate exhibit a complex fractal-like shape [22, 23, 26–29, 33–37]. From the perspective of the kinetic deposition process of the admolecules, the shape of the island is determined by the edge diffusion constant (D_{edg}) versus the surface diffusion constant (D_s) ratio (D_{edg}/D_s) [45–47]. A low D_{edg}/D_s tends to give rise to a complex shape, such as a fractal. Therefore, if D_s determines N, as mentioned above, the D_{edg} values of different materials having the same N value could potentially be compared based on the shape of the 2D islands. DPh-DNTT 2D islands retain their compact round shape during growth. As a result, an increase in nominal thickness leads to the formation of large isolated compact islands with a diameter of about 4 μm [40], where N is approximately 0.1 μm^{-2}. These large and compact 2D islands present the benefit of potentially suppressing carrier scattering at the grain boundaries in FETs. By contrast, pentacene 2D islands with a similar N value have been reported to exhibit complex fractal-like shapes [22, 26, 27, 33], suggesting that D_{edg} is larger for DPh-DNTT than for pentacene. For DPh-DNTT, active mobile admolecules at the edge, with a higher $D_{edg,}$ may aggregate at the kink sites to give 2D islands with a compact shape.

Moreover, the growth process of the second layer was also investigated. **Figure 3** shows the optical dark-field microscopy and AFM images of the films deposited at 160 °C on the substrates treated with UV-O_3 **Fig. 3(a)** and O_2 plasma **Fig. 3(b)**, with a nominal thickness of 4.8 and 3.6 nm, respectively. The AFM image corresponds to the dotted area in **Fig. 3(b)**. The height diagrams of the film for the three dotted lines (A-A', B-B', C-C') in the AFM image were indicated on the AFM image, respectively. Based on the evolution of the 2D island growth for the first layer, two 2D islands coalesced into one island. Some coalesced regions can be seen smoothly connected in **Fig. 3(c)** at the AFM resolution. In addition, nucleation of a second layer can be observed as a flat 2D island deposited on the first layer

before completion of the first layer. When focusing on the number of nuclei for the second layer, we concluded that N for the second layer is smaller than N for the first layer. Note that the elongated parts in both images are DPh-DNTT formations with a height of more than 80 nm, much taller than the remaining area. These formations may be tall walls, also observed in previous studies [12, 18]. The formations tend to appear during the growth of the second layer. To support these observations, it seems that the tall wall in the AFM image (C-C') elongates from the second layer part (B-B').

Furthermore, the thick film surface was investigated. **Figure 4** shows the optical bright-field microscopy **Fig. 4(a)** and AFM **Fig. 4(b)** images of the surface of a DPh-DNTT film deposited at 160 °C on a substrate treated with UV-O_3. The nominal thickness of the films was 25 nm. The image color contrast was strongly enhanced by image processing. These figures show the formation on the top layer of flat 2D islands with fractal-like shapes. Interestingly, similar morphologies were observed irrespective of surface treatment [40]. These experimental results suggest a layer-by-layer growth mode.

The shape and nucleation density of the 2D islands deposited on the top layer, shown in **Fig. 4,** are different from those of the 2D islands in the first layer. This difference is probably due to the fact that the DPh-DNTT molecules interact differently with the SiO_2 substrate and the DPh-DNTT layer, since the first layer grows on the SiO_2 substrate, while the subsequent layers grow on a DPh-DNTT layer, affecting admolecular dynamics. Let us discuss the kinetics of admolecular diffusion again using D_s and D_{edg}. Since the shape of the 2D islands at the top layer evolves to a complex fractal, D_{edg}/D_s for the top layer is probably lower. If the D_{edg} is assume to be independent of base material, the D_s for the second or subsequent layer higher than that for the first layer. Since D_{edg} mainly depends on the intermolecular interactions, the assumption for D_{edg} is natural. As a result, nucleation density for the upper

layers must be lower with respect to the first layer, which is consistent with the observation in this study.

In order to confirm a layer-by-layer growth mode, the edge of the film was patterned with a shadow mask (**Fig. 5(a)**) and observed using the same techniques. **Figure 5(b) and (c)** show the optical bright-field microscopy and AFM images, respectively, of the 25-nm-thick DPh-DNTT film deposited at 160 °C on the substrate treated with O_2 plasma. The AFM image corresponds to the dotted line region in **Fig. 5(b)**. From the AFM height image, the step-terrace structure from the first layer to the 6th layer was clearly visible. Therefore, we concluded that the DPh-DNTT film was formed according to a layer-by-layer growth mode. Furthermore, the optical microscopy image exhibits a similar pattern with different colors. The correspondence indicates that the number of layers in a film with a layer-by-layer structure can be easily estimated from the color differences in the optical microscopy image. Based on the colors identified in the AFM height image, the film is comprised of 5 to 6 layers. The flat morphology of the DPh-DNTT films is quite different from that of pentacene films, in which dendritic mounds form on the surface [25, 26, 29, 31, 32]. The walls protruding from the surface seen in **Fig. 3** appear in the thick film as the black lines in **Fig. 4(a)** and the yellow lines in image **Fig.5 (b)**, respectively, which should be restrained from the view point of carrier transport in the FETs. Therefore, further investigations to control and clarify the growth mechanism for the tall walls in the early stage are required.

Figure 6 shows the Raman spectra for the monolayer and 5–6-layer DPh-DNTT films deposited on the substrate treated with O_2 plasma. The thicker film corresponds to the sample shown in **Fig. 5 (b)**. Although the film includes tall walls, the imaged region will not show them since the resolution of the Raman measurement (~1 μm) is smaller than the spatial distribution of the walls. For the DPh-DNTT film having 5–6 layers, several peaks were observed in the measured range, with the peak at 1393 cm^{-1} being the most intense. Although

the spectrum for the monolayer film is very weak as compared to that for the 5–6-layer film, it also exhibits the peak at 1393 cm^{-1}. The integral intensity of the peak at 1393 cm^{-1} for the monolayer film is approximately one-fourth to one-sixth of the integral intensity for the 5–6-layer film. Thus, we can also estimate the approximate number of layers in the film from the integral intensity of this peak.

CONCLUSION

In this study, the growth mechanism of DPh-DNTT films was investigated by observing few-nanometer thick films growing on a SiO_2 substrate. A layer-by-layer growth mode was confirmed by AFM. In the early stages of growth, flat 2D islands with a thickness of about 2.3 nm formed and grew on the substrate, where molecules stand vertically. After formation of the first layer, subsequent layers grow in the same manner. Since films grown according to a layer-by-layer growth mode exhibit a clear height difference between layers with a known thickness, color differences corresponding to the different layers could be clearly seen in the optical microscopy images. This allows easy evaluation of the film morphology and estimation of the number of layers within the film. The effects of T_s and the pre-treatment of the SiO_2 substrate on N for the first layer was also investigated by optical microscopy. The results show that N decreases with UV-O_3 or O_2 plasma treatment of the substrate or with increase of T_s, resulting in large 2D islands. The deposited thin films were also characterized by micro-Raman. An intense peak at 1393 cm^{-1} was observed for both the monolayer and multilayer films, allowing estimation of the number of layers based on peak intensity. In contrast to well-studied pentacene films, the 2D islands in DPh-DNTT films exhibit a compact round shape with a large size. On the other hand, subsequent layers are not affected by the treatment of the SiO_2 substrate because they form on the previous DPh-DNTT layer. In the layer-by-layer growth mode, 2D islands with fractal shapes formed on the top layer with a

smaller nucleation density. These differences are a consequence of the different diffusion coefficients on the various base materials (SiO_2 substrate versus subsequent DPh-DNTT layers). The findings of the present study allow to control and predict the growth behavior of organic molecules with an elongated shape containing side chains, which will be relevant for electronic applications.

FIGURES

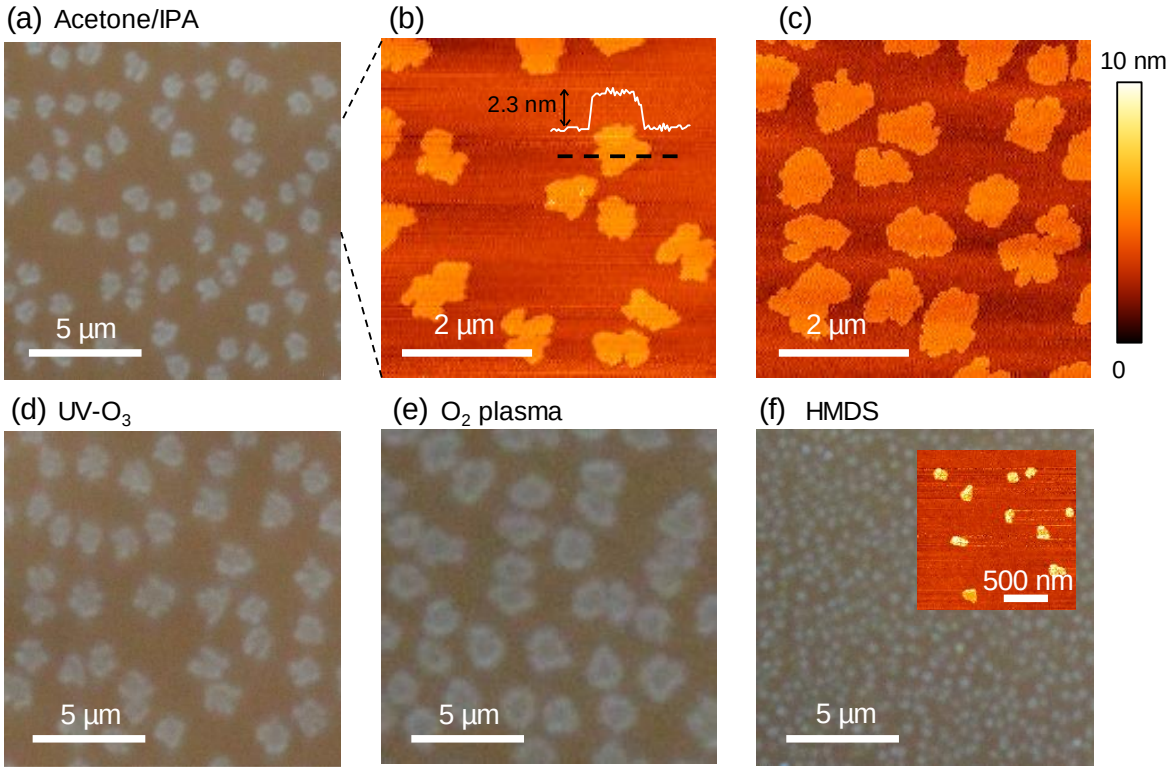

Figure 1: Dark-field optical microscopy and AFM images of 2D islands deposited at 160 °C on surfaces submitted to different treatments. The nominal thicknesses of the films are 1.2 nm **(a, b, d-f)** and 2.4 nm **(c)**. The color bar applies to all AFM images. Fig. **(a–c)** show the growth evolution of 2D islands on a substrate cleaned with acetone/IPA. AFM image **(b)** is the observation of the same sample for **(a)**. The sample for **(c)** is different. The inset diagram in **(b)** shows the height of the 2D island on the dotted line. The 2D islands grow isotropically without new nucleation. The bottom three images show the 2D islands deposited on the substrates treated with UV-O_3 **(d)**, O_2 plasma **(e)**, and HMDS **(f)**, respectively. HMDS treatment increases N of the 2D islands. By contrast, UV-O_3 and O_2 plasma treatment decreases N, resulting in large 2D islands. The inset image in **(f)** is the AFM image of the same sample, where N of AFM image corresponds to N of the optical microscopy image.

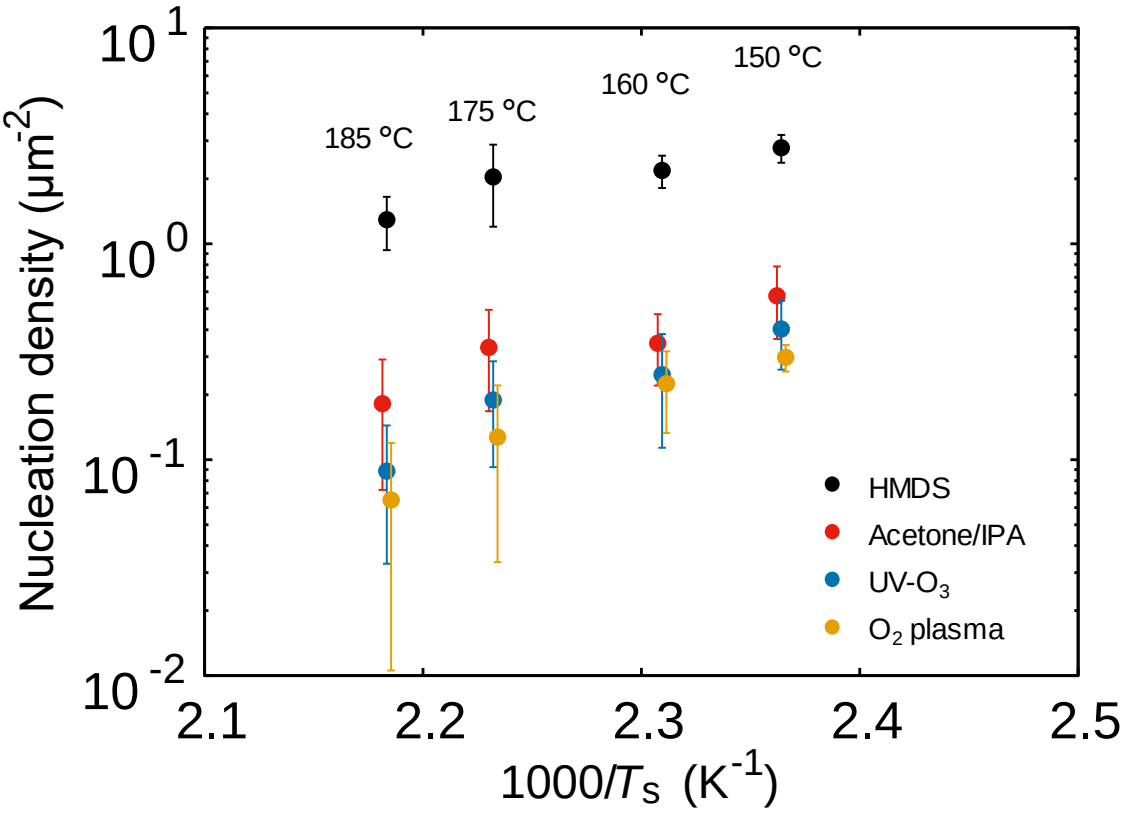

Figure 2: Nucleation density as a function of the inverse of the substrate temperature for the different surface treatments. We can observe that N decreases exponentially as T_s increases irrespective of surface treatment. The plots depict the average N value for the samples, with the error bars indicating the standard deviation. More than three samples were evaluated to obtain the values.

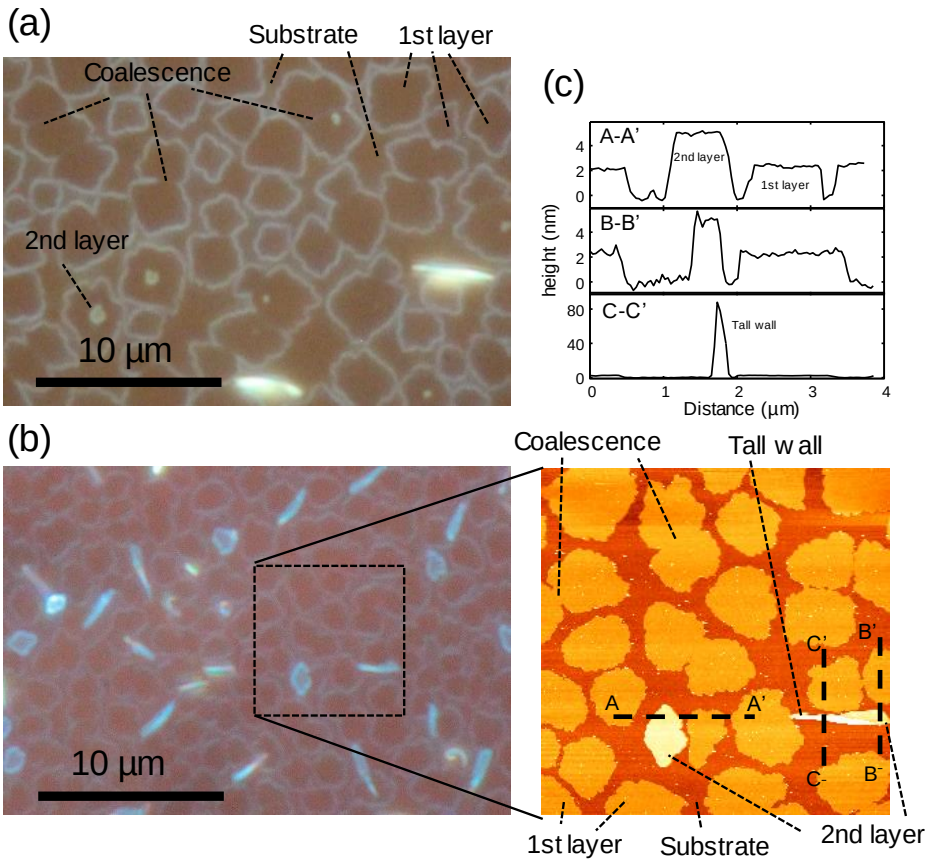

Figure 3: Evolution of the 2D islands on the first layer and nucleation on the second layer. The films deposited at 160 °C on the substrates treated with UV-O_3 **(a)** and O_2 plasm **(b, c)** have nominal thicknesses of 4.8 and 3.6 nm, respectively, as observed by optical microscopy and AFM. The AFM image corresponds to the dotted region in **(b)**. The top figure of **(c)** shows the height diagrams for the three dotted lines (A-A', B-B', C-C') in the AFM image. The substrate exposed area, the first and second layers, and the coalesced regions are labeled. The smooth connection of some 2D islands could be detected at the AFM resolution level. In all images, the elongated parts are tall walls of DPh-DNTT molecules with a height of more than 80 nm, which often appear in DNTT and DNTT derivative thin films. These walls were formed in the early stage of growth.

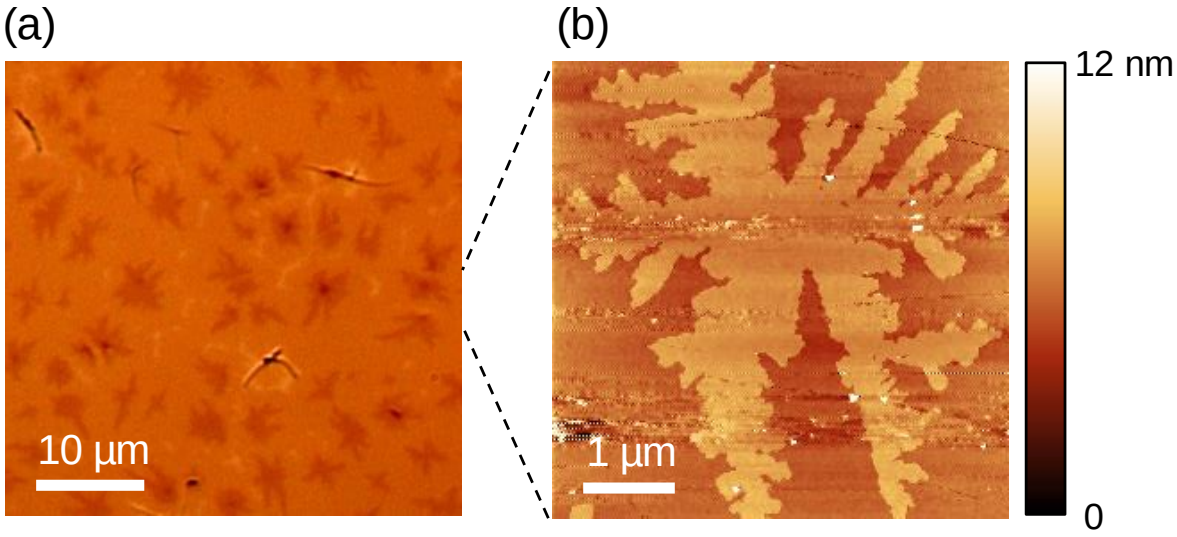

Figure 4: Optical bright-field microscopy **(a)** and AFM **(b)** images of the surfaces of the films deposited at 160 °C on a substrate treated with UV-O_3. The nominal thickness of the films was 25 nm. The image color contrast was strongly enhanced by image processing. The flat 2D islands with a fractal shape were formed on the top layer, suggesting a layer-by-layer growth. The nucleation density and the shape of the 2D islands deposited on the top layer is clearly different with respect to the first layer.

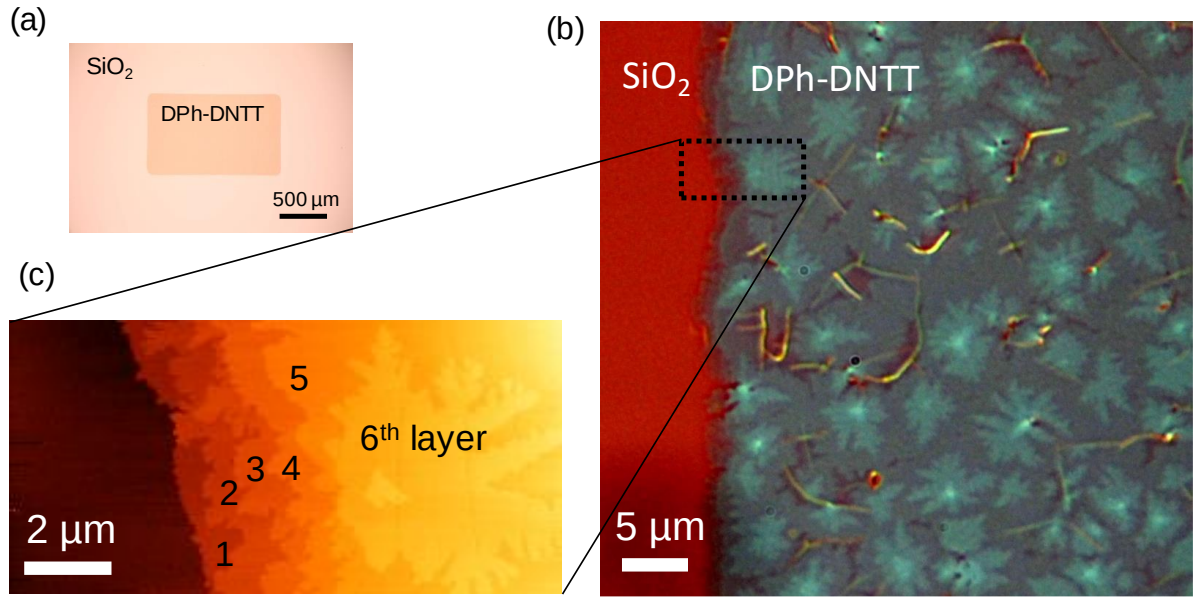

Figure 5: Images of the edge of a film patterned with a metal shadow mask. Fig. **(a)** shows a typical patterned film. Fig. **(b)** and **(c)** show the optical bright-field microscopy and AFM images, respectively, for the films deposited at 160 °C on the substrate treated with O_2 plasma. The nominal thickness of the films was 25 nm. The color contrast in the image obtained by optical microscopy was strongly enhanced by image processing. The AFM image **(c)**, which corresponds to the dotted region in **(b)**, shows a clear step-terrace structure from the first to the sixth layer, as identified from the different colors in the image. The shape of the islands on the top layer can also be appreciated in the optical microscopy image. The yellow lines in image **(b)** represent tall DPh-DNTT walls protruding from the surface.

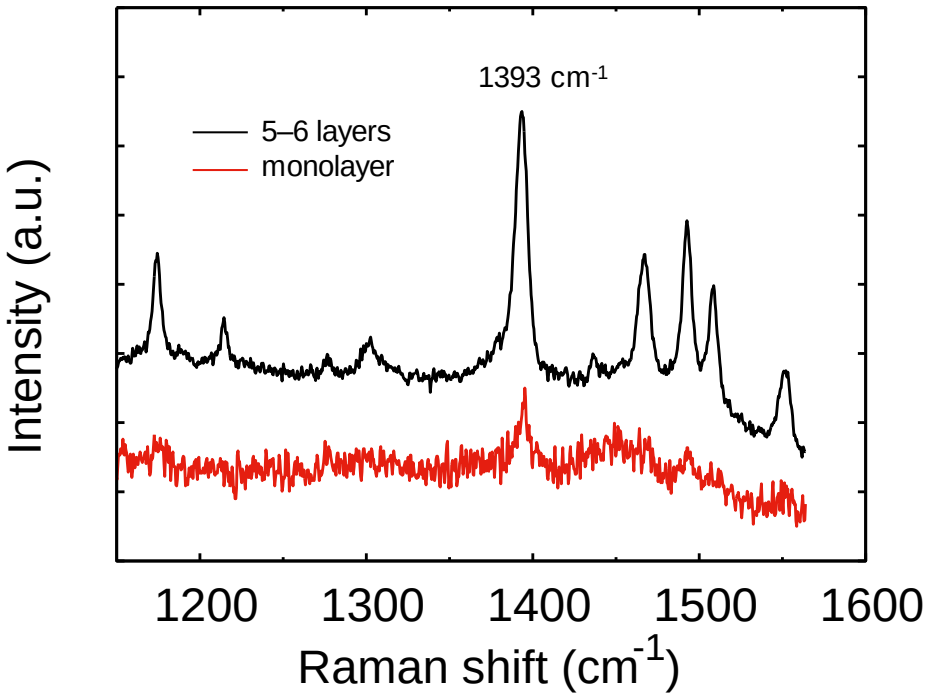

Figure 6: Raman spectra for multilayer (black) and monolayer (red) films deposited on the substrates treated with O_2 plasma. Since the multilayer film corresponds to the sample shown in **Fig. 5(b)**, the obtained data are for 5 to 6 layers. The strongest peak, at 1393 cm^{-1}, was also observed for the monolayer film.

SUPPLEMENTARY MATERIALS

The comparison of the optical bright-field and dark-field microscopy images, the quantum chemical calculations to determine the length of the DPh-DNTT molecule, the images of large 2D islands in the monolayer, the images of thick films deposited on the substrates cleaned with acetone/IPA and treated with HMDS, and comparison between measured Raman spectra and vibrational mode calculations are shown in the Supplementary Materials.

ACKNWLEDGEMENTS

This work was supported by the Leading Initiative for Excellent Young Researcher (LEADER) of the Ministry of Education, Culture, Sports, Science and Technology in Japan and JSPS KAKENHI Grant Numbers 19H02171, 19K15048. The authors would like to thank Nippon Kayaku Co., Ltd. for supplying DPh-DNTT.

NOTES

The authors declare no competing financial interests.

REFERENCES

[1] Yokota, T., Kuribara, K., Tokuhara, T., Zschieschang, U., Klauk, H., Takimiya, K., ... & Someya, T. (2013). Flexible Low‐Voltage Organic Transistors with High Thermal Stability at 250 C. Advanced materials, 25(27), 3639-3644.

[2] Kang, M. J., Miyazaki, E., Osaka, I., Takimiya, K., & Nakao, A. (2013). Diphenyl derivatives of dinaphtho[2,3-*b*:2',3'-*f*]thieno[3,2-*b*]thiophene: organic semiconductors for thermally stable thin-film transistors. ACS applied materials & interfaces, 5(7), 2331-2336.

[3] Kang, M. J., Doi, I., Mori, H., Miyazaki, E., Takimiya, K., Ikeda, M., & Kuwabara, H. (2011). Alkylated Dinaphtho[2,3-*b*:2',3'-*f*]Thieno[3,2-*b*]Thiophenes (Cn‐DNTTs): Organic Semiconductors for High‐Performance Thin‐Film Transistors. Advanced Materials, 23(10), 1222-1225.

[4] Xie, W., Willa, K., Wu, Y., Häusermann, R., Takimiya, K., Batlogg, B., & Frisbie, C. D. (2013). Temperature‐Independent Transport in High‐Mobility Dinaphtho‐Thieno‐Thiophene (DNTT) Single Crystal Transistors. Advanced Materials, 25(25), 3478-3484.

[5] Haas, S., Takahashi, Y., Takimiya, K., & Hasegawa, T. (2009). High-performance dinaphtho-thieno-thiophene single crystal field-effect transistors. Applied Physics Letters, 95(2), 022111.

[6] Yamamoto, T., & Takimiya, K. (2007). Facile synthesis of highly π-extended heteroarenes, dinaphtho[2,3-*b*:2',3'-*f*]chalcogenopheno[3,2-*b*]chalcogenophenes, and their application to field-effect transistors. Journal of the American Chemical Society, 129(8), 2224-2225.

[7] Zschieschang, U., Ante, F., Kälblein, D., Yamamoto, T., Takimiya, K., Kuwabara, H., ... & Klauk, H. (2011). Dinaphtho[2,3-*b*:2',3'-*f*]thieno[3,2-*b*]thiophene (DNTT) thin-film transistors with improved performance and stability. Organic Electronics, 12(8), 1370-1375.

[8] Northrup, J. E., Xie, W., Sun, Y. Y., & Zhang, S. (2013). Electronic Structure and Mobility of Alkylated and Nonalkylated Organic Semiconductors: Role of van der Waals Interactions. Applied Physics Express, 6(7), 071601.

[9] Uemura, T., Nakayama, K., Hirose, Y., Soeda, J., Uno, M., Li, W., ... & Takeya, J. (2012). Band-like transport in solution-crystallized organic transistors. Current Applied Physics, 12, S87-S91.

[10] Ou-Yang, W., Uemura, T., Miyake, K., Onish, S., Kato, T., Katayama, M., ... & Hamada, M. (2012). High-performance organic transistors with high-k dielectrics: A comparative

study on solution-processed single crystals and vacuum-deposited polycrystalline films of 2, 9-didecyl-dinaphtho[2,3-*b*:2',3'-*f*]thieno[3,2-*b*]thiophene. Applied Physics Letters, 101(22), 223304.

[11] Nakayama, K., Hirose, Y., Soeda, J., Yoshizumi, M., Uemura, T., Uno, M., ... & Miyazaki, E. (2011). Patternable solution‐crystallized organic transistors with high charge carrier mobility. Advanced Materials, 23(14), 1626-1629.

[12] Hofmockel, R., Zschieschang, U., Kraft, U., Rödel, R., Hansen, N. H., Stolte, M., ... & Klauk, H. (2013). High-mobility organic thin-film transistors based on a small-molecule semiconductor deposited in vacuum and by solution shearing. Organic Electronics, 14(12), 3213-3221.

[13] Matsumoto, T., Ou-Yang, W., Miyake, K., Uemura, T., & Takeya, J. (2013). Study of contact resistance of high-mobility organic transistors through comparisons. Organic Electronics, 14(10), 2590-2595.

[14] Niimi, K., Kang, M. J., Miyazaki, E., Osaka, I., & Takimiya, K. (2011). General Synthesis of Dinaphtho[2,3-*b*:2',3'-*f*]thieno[3,2-*b*]thiophene (DNTT) Derivatives. Organic letters, 13(13), 3430-3433.

[15] Tsurumi, J., Amin, A. Y., Okamoto, T., Mitsui, C., Takimiya, K., Matsui, H., ... & Takeya, J. (2014). Solution-processed single-crystalline organic transistors on patterned ultrathin gate insulators. Organic Electronics, 15(6), 1184-1188.

[16] Kraft, U., Takimiya, K., Kang, M. J., Rödel, R., Letzkus, F., Burghartz, J. N., ... & Klauk, H. (2016). Detailed analysis and contact properties of low-voltage organic thin-film transistors based on dinaphtho[2,3-*b*:2',3'-*f*]thieno[3,2-*b*]thiophene (DNTT) and its didecyl and diphenyl derivatives. Organic Electronics, 35, 33-40.

[17] Kim, C. H., Thomas, S., Kim, J. H., Elliott, M., Macdonald, J. E., & Yoon, M. H. (2018). Potentiometric Parameterization of Dinaphtho[2,3-*b*:2',3'-*f*]thieno[3,2-*b*]thiophene

Field‐Effect Transistors with a Varying Degree of Nonidealities. Advanced Electronic Materials, 4(7), 1700514.

[18] Doi, I., Kang, M. J., & Takimiya, K. (2012). High mobility organic thin-film transistors on plastic substrate. Current Applied Physics, 12, e2-e5.

[19] Kraft, U., Sejfić, M., Kang, M. J., Takimiya, K., Zaki, T., Letzkus, F., ... & Klauk, H. (2015). Flexible Low‐Voltage Organic Complementary Circuits: Finding the Optimum Combination of Semiconductors and Monolayer Gate Dielectrics. Advanced Materials, 27(2), 207-214.

[20] Breuer, T., Karthäuser, A., Klemm, H., Genuzio, F., Peschel, G., Fuhrich, A., Schmidt, T. and Witte, G., (2017). Exceptional Dewetting of Organic Semiconductor Films: The Case of Dinaphthothienothiophene (DNTT) at Dielectric Interfaces. ACS applied materials & interfaces, 9(9), 8384-8392.

[21] Ruiz, R., Papadimitratos, A., Mayer, A. C., & Malliaras, G. G. (2005). Thickness Dependence of Mobility in Pentacene Thin‐Film Transistors. Advanced Materials, 17(14), 1795-1798.

[22] Pratontep, S., Nüesch, F., Zuppiroli, L., & Brinkmann, M. (2005). Comparison between nucleation of pentacene monolayer islands on polymeric and inorganic substrates. Physical Review B, 72(8), 085211.

[23] Ribič, P. R., Kalihari, V., Frisbie, C. D., & Bratina, G. (2009). Growth of ultrathin pentacene films on polymeric substrates. Physical Review B, 80(11), 115307.

[24] Killampalli, A. S., & Engstrom, J. R. (2006). Nucleation of pentacene thin films on silicon dioxide modified with hexamethyldisilazane. Applied physics letters, 88(14), 143125.

[25] Tejima, M., Kita, K., Kyuno, K., & Toriumi, A. (2004). Study on the growth mechanism of pentacene thin films by the analysis of island density and island size distribution. Applied physics letters, 85(17), 3746-3748.

[26] Stadlober, B., Haas, U., Maresch, H., & Haase, A. (2006). Growth model of pentacene on inorganic and organic dielectrics based on scaling and rate-equation theory. Physical Review B, 74(16), 165302.

[27] Pratontep, S., Brinkmann, M., Nüesch, F., & Zuppiroli, L. (2004). Nucleation and growth of ultrathin pentacene films on silicon dioxide: effect of deposition rate and substrate temperature. Synthetic Metals, 146(3), 387-391.

[28] Conrad, B. R., Gomar-Nadal, E., Cullen, W. G., Pimpinelli, A., Einstein, T. L., & Williams, E. D. (2008). Effect of impurities on pentacene island nucleation. Physical Review B, 77(20), 205328.

[29] Killampalli, A. S., Schroeder, T. W., & Engstrom, J. R. (2005). Nucleation of pentacene on silicon dioxide at hyperthermal energies. Applied Physics Letters, 87(3), 033110.

[30] Virkar, A., Mannsfeld, S., Oh, J. H., Toney, M. F., Tan, Y. H., Liu, G. Y., ... & Bao, Z. (2009). The role of OTS density on pentacene and C_{60} nucleation, thin film growth, and transistor performance. Advanced Functional Materials, 19(12), 1962-1970.

[31] Kalb, W., Lang, P., Mottaghi, M., Aubin, H., Horowitz, G. and Wuttig, M., (2004). Structure–performance relationship in pentacene/Al_2O_3 thin-film transistors. Synthetic Metals, 146(3), pp.279-282.

[32] Yang, S.Y., Shin, K. and Park, C.E., (2005). The effect of gate‐dielectric surface energy on pentacene morphology and organic field‐effect transistor characteristics. Advanced functional materials, 15(11), pp.1806-1814.

[33] Pratontep, S., Brinkmann, M., Nüesch, F., & Zuppiroli, L. (2004). Correlated growth in ultrathin pentacene films on silicon oxide: effect of deposition rate. Physical Review B, 69(16), 165201.

[34] Wu, Y., Toccoli, T., Zhang, J., Koch, N., Iacob, E., Pallaoro, A., ... & Rudolf, P. (2009). Key role of molecular kinetic energy in early stages of pentacene island growth. Applied Physics A, 95(1), 21-27.

[35] Ruiz, R., Nickel, B., Koch, N., Feldman, L. C., Haglund, R. F., Kahn, A., & Scoles, G. (2003). Pentacene ultrathin film formation on reduced and oxidized Si surfaces. Physical Review B, 67(12), 125406.

[36] Zu Heringdorf, F. J. M., Reuter, M. C., & Tromp, R. M. (2004). The nucleation of pentacene thin films. Applied Physics A, 78(6), 787-791.

[37] Al‐Mahboob, A., Fujikawa, Y., Sakurai, T., & Sadowski, J. T. (2013). Real‐Time Microscopy of Reorientation Driven Nucleation and Growth in Pentacene Thin Films on Silicon Dioxide. Advanced Functional Materials, 23(20), 2653-2660.

[38] Blake, P., Hill, E. W., Castro Neto, A. H., Novoselov, K. S., Jiang, D., Yang, R., ... & Geim, A. K. (2007). Making graphene visible. Applied physics letters, 91(6), 063124.

[39] Kitani, A., Kimura, Y., Kitamura, M., & Arakawa, Y. (2016). Threshold voltage control in dinaphthothienothiophene-based organic transistors by plasma treatment: Toward their application to logic circuits. Japanese Journal of Applied Physics, 55(3S2), 03DC03.

[40] Hattori, Y., Kimura, Y., Yoshioka, T., and Kitamura, M., (2019) Data on optical microscopy and vibrational modes in Diphenyl Dinaphthothienothiophene thin films, data in brief, *submitted*.

[41] Venable, J. A., Spiller, G. D. T., & Hanbucken, M. (1984). Nucleation and growth of thin film. Rep. Prog. Phys., 47(4), 399-459.

[42] Bartelt, M. C., & Evans, J. W. (1992). Scaling analysis of diffusion-mediated island growth in surface adsorption processes. Physical Review B, 46(19), 12675.

[43] Bales, G. S., & Chrzan, D. C. (1994). Dynamics of irreversible island growth during submonolayer epitaxy. Physical Review B, 50(9), 6057.

[44] Stroscio, J. A., & Pierce, D. T. (1994). Scaling of diffusion-mediated island growth in iron-on-iron homoepitaxy. Physical Review B, 49(12), 8522.

[45] Bales, G. S., & Chrzan, D. C. (1995). Transition from compact to fractal islands during submonolayer epitaxial growth. Physical review letters, 74(24), 4879.

[46] Pimpinelli, A., & Ferrando, R. (1999). Reentrant morphological instability of epitaxial islands. Physical Review B, 60(24), 17016.

[47] Saito, Y. (2003). Two-dimensional nucleation with edge and corner diffusions. Journal of the Physical Society of Japan, 72(8), 2008-2014.